Iurchenkova, A. A.; Kallio, T.; Fedorovskaya, E. O.

Relationships between polypyrrole synthesis conditions, its morphology and electronic structure with supercapacitor properties measured in electrolytes with different ions and pH values

Published in:
Electrochimica Acta

DOI:
10.1016/j.electacta.2021.138892

Published: 20/09/2021

Document Version
Peer-reviewed accepted author manuscript, also known as Final accepted manuscript or Post-print

Please cite the original version:
Iurchenkova, A. A., Kallio, T., & Fedorovskaya, E. O. (2021). Relationships between polypyrrole synthesis conditions, its morphology and electronic structure with supercapacitor properties measured in electrolytes with different ions and pH values. *Electrochimica Acta*, *391*, Article 138892.
https://doi.org/10.1016/j.electacta.2021.138892

Relationships between polypyrrole synthesis conditions, its morphology and electronic structure with supercapacitor properties measured in electrolytes with different ions and pH value

Iurchenkova A.A.[a,b,*], *Kallio T.*[b], *Fedorovskaya E.O.*[b]

[a]Novosibirsk State University, Laboratory of hybrid materials for electrochemical energy storage devices, Pirogova st. 1, Novosibirsk, 630090, Russia.

[b]Research Group of Electrochemical Energy Conversion, Department of Chemistry, School of Chemical Engineering, Aalto University, P.O. Box 16100, FI-00076, Finland.

* anna.yurchenkova@yandex.ru

Abstract

Despite a large number of articles about synthesis methods, structure, morphology and electrochemical properties of polypyrrole, none of these works reports the relationships between polypyrrole synthetic conditions, the electronic states of atoms in the polymer chains and its electrochemical properties in various electrolytes. Our work is dedicated to filling part of this gap. This work is focused on the effect of the synthetic medium used for polypyrrole synthesis on their atomic and electronic structure and morphology as well as investigation of the influence of these on the electrochemical characteristics of polypyrrole in aqueous electrolytes with different ions and pH values within a supercapacitor setup. It is shown that synthetic medium does not affect polymer particle shapes but changes particle sizes. Using oxygen functional groups containing synthetic medium based on water and ethanol leads to a decrease in C:N ratio, increase in C:O ratio, increase in the concentration of positively charged nitrogen-species and formation of linear-structured polymer chains. Contrary, acetonitrile-based synthetic medium without oxygen-containing functional groups leads to an increase in C:N ratio and concentration of neutrally charged nitrogen species, decrease in C:O ratio and formation of branched-structured polymer chains. Electrochemical properties of polypyrrole depend on the nature of the electrolyte, then nitrogen species and oxygen-containing functional groups in polypyrrole structure, and the size of polypyrrole particles. The favorable electrolyte for using polypyrrole in supercapacitors is neutral. The specific capacitance of polypyrrole produced in acetonitrile is shown to reach the value of ~ 385 F g $^{-1}$ which is stable for more than 10,000 cycles in 1M KCl aqueous solution.

Graphical abstract:

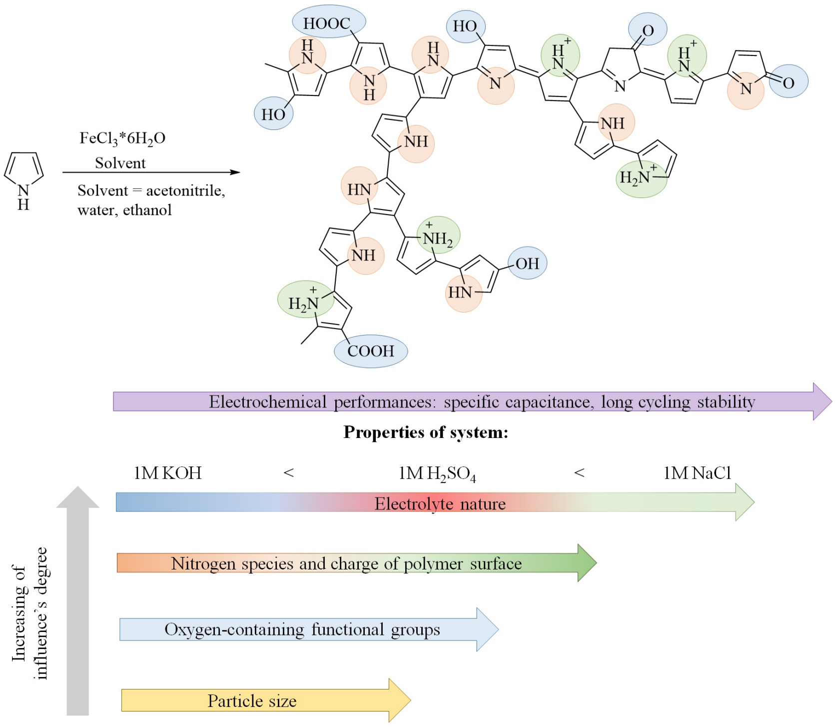

Keywords: Supercapacitors, polypyrrole, FTIR, XPS, electronically conducting polymer, aqueous electrolytes

1. Introduction

Due to their small size, high power density, high long term cycling stability, and high charge-discharge rates, supercapacitors (SCs) are promising devices for energy storage. [1–4] Such important characteristics of SCs as stability during long term cycling, specific capacitances, and the wide electrochemical window strongly depend on the electrode materials. Carbon nanomaterials [5–7], transition metal oxides [8,9], MAX-phase (a class of 2D materials with the formula $M_{n+1}AX_n$, where M is a transition metal, A is an element of the III-VI groups of the periodic table and X is a carbon and/or nitrogen atoms) and MXenes (a class of graphene-like layered materials with 2D structure obtained by exfoliation of MAX-phase compounds) [10], and conducting polymers (CPs) [11,12] are widely used as electrode materials of SCs. In recent years, CPs have attracted a lot of attention in the field of creating SCs with unique properties such as flexibility and high voltage operating range. The functioning of CPs in different media is possible due to their mixed conduction mechanism, branched porous structure, the ability to control morphology during synthesis and the ability to function in non-aqueous media. In addition to the use of CPs as electrode materials, they are also widely used in such areas as drug delivery systems [13], Li-ion batteries [14], transistors [15], OLED [16], fuel cells [17], etc.

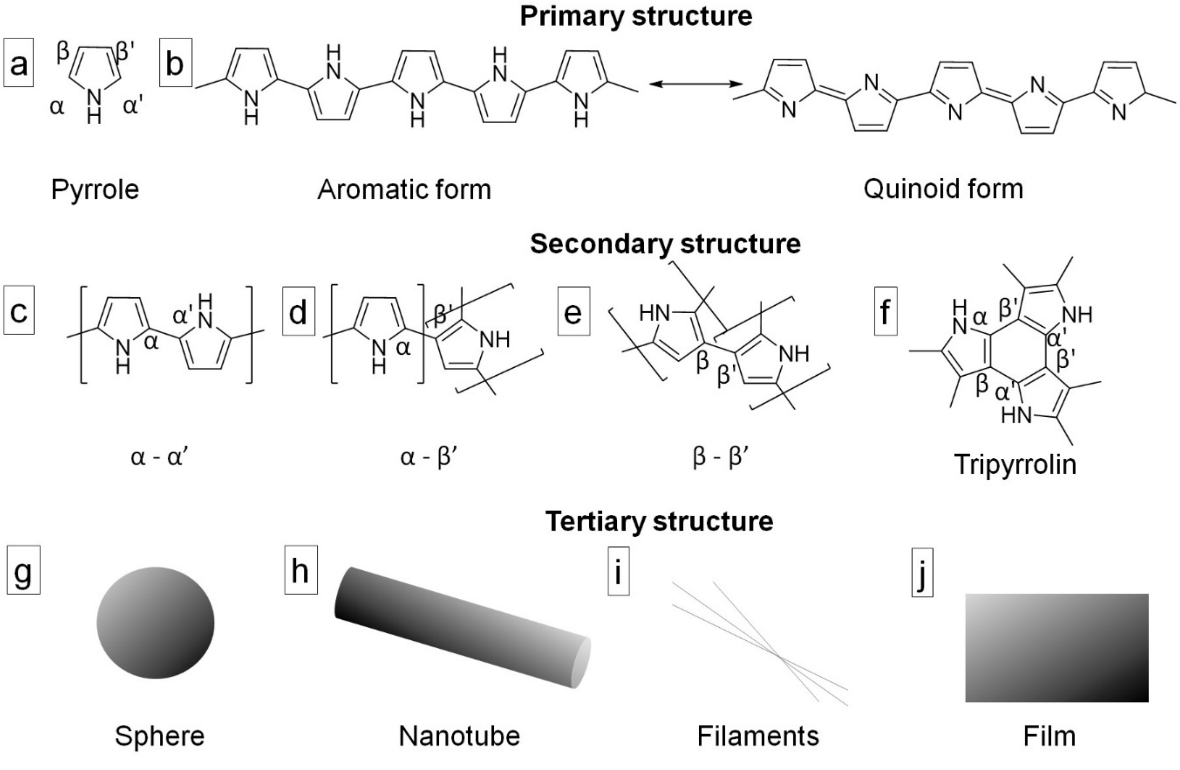

Figure 1. Primary, secondary, and tertiary structures of PPy.

Polypyrrole (PPy) is one of the most studied polymers in recent years, due to its unique conducting mechanism. Unlike other CPs, the conductivity of PPy weakly depends on the protonation level (in comparison to polyaniline) and is mainly determined by the chemical and electronic structure. It is well-known that the structure of materials affects their physical and chemical properties, especially in nanomaterials [18]. The chemical structure of PPy depends on the synthesis method and conditions. Pyrrole monomer is a N-containing pentagon with four carbon atoms and one nitrogen atom in the structure. In this case, there are two non-equivalent carbon atom groups. The first group of carbon atoms is located near the nitrogen atom and occupies α-positions of the pyrrole rings, the second one consists of atoms connected to carbon atoms only and is called the β-position of the pyrrole ring (Figure 1a). The primary or ideal structure of PPy is represented by repeated pyrrole units in their aromatic and/or quinoid form [19] (Figure 1b). Secondary PPy structure is mainly represented by α-α' connected units (Figure 1c), less often by α-β' (Figure 1d) or β-β' (Figure 1e) connected units [20]. Tertiary PPy structure is amorphous, sometimes with low crystallinity regions, where polymer rings are oriented in a co-planar manner. Tripirrolin subunits are sometimes found in the secondary and tertiary PPy structures (Figure 1f). In terms of micro/nanostructure, PPy can be classified into three types with different dimensions [21]: Zero-dimensional nano-particles (Figure 1g); one-dimensional nanowires, nanotubes (Figure 1h), nanofibers, nanoribbons (Figure 1i); two-dimensional nanosheets (Figure 1j); three-dimensional porous hydrogels.

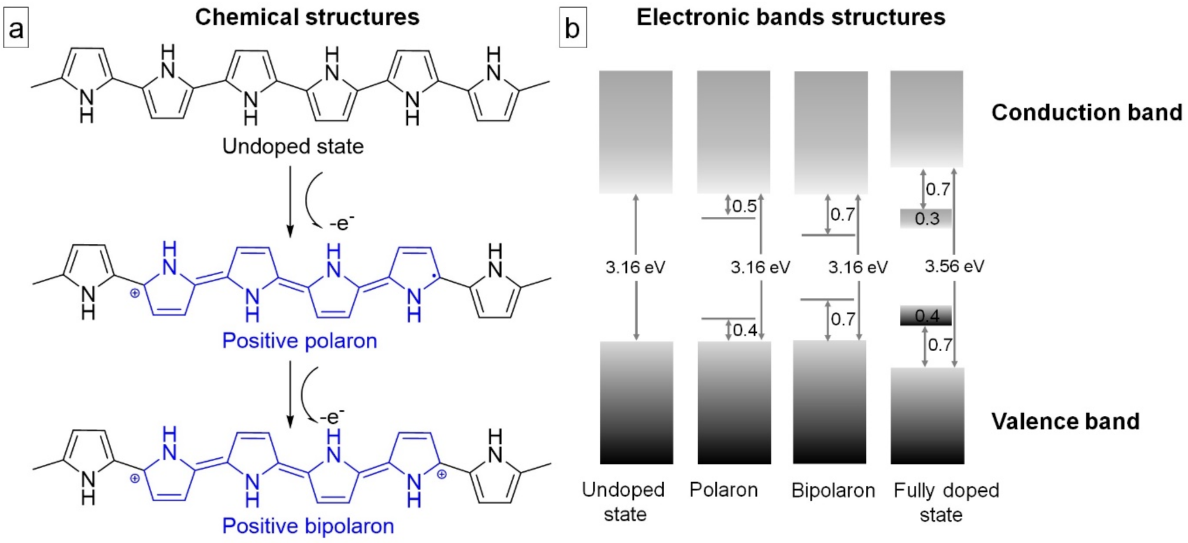

Figure 2. Chemical and electronic band structures of PPy in different doping states.

Charge transfer in PPy occurs due to the formation of such quasiparticles as polarons and bipolarons (Figure 2a). PPy is an insulator in its normal structure (fully black-colored polymer chain in Figure 2a) with a large band gap of ~ 3.16 eV (Figure 2b). When one π-electron is removed from the PPy chain, structural deformation of pyrrole ring with the transition from benzenoid to quinoid structure occurs with polaron quasi-particle formation [22]. This leads to the appearance of two localized electronic levels in the band gap. At the same time, the unpaired electron occupies the bonding state. When the second electron is removed from the PPy chain during proceeding oxidation, the formation of a bipolaron occurs with stronger benzoid-to-quinoid deformation (Figure 2a) than one in polaron [23]. If the polymer is further oxidized, the formation of narrow bipolaronic bands occurs, leading to the decrease in the energy gap from 3.16 to 1.4 eV [24] (Figure 2b).

There are many synthesis methods of PPy which can be divided into chemical, electrochemical, and physical methods. Those methods differ both in the nature of the polymerizing agent and the polymerization mechanism. Chemical polymerization of pyrrole is the easy, user-friendly, and well-scaled method for PPy synthesis. Moreover, chemical polymerization of PPy can be done in an aqueous and non-aqueous medium (ionic liquids, organic solvents), under ambient conditions [25]. This synthesis method needs from 10 to 60 minutes for full polymerization, wherein the conversion of pyrrole into PPy is practically complete. Inorganic transition metal salt solutions [26,27] ($FeCl_3$, $AlCl_3$, $Ag(NO_3)_2$, $Cu(NO_3)_2$, $Cu(NO_3)_2$-$AlCl_3$ etc.) or peroxides (benzoyl peroxide [28], $NH_4S_2O_8$) may be used as chemical oxidants in this processes. The main disadvantage of the chemical synthesis is the termination of the growing polymer chain with the incorporation of oxygen-containing functional groups. [29,30]

Comparing with the chemical methods, electrochemical synthesis has some unique advantages. Electrochemical polymerization allows controlling conductivity, morphology, mass and thickness of the deposited PPy film. Moreover, this type of synthesis can be used for covering other materials with thin polymer films [21]. Furthermore, this method is suitable for the synthesis of small amounts of polymer on substrates not exceeding 2×2 cm in size. Physical methods of PPy synthesis include chemical vapor deposition (CVD) [31], plasma-induced polymerization [32], self-assembly [33], and spin-coating [34] methods.

The electrochemical activity of CPs is different from other SC electrode materials. Firstly, it is shown that thermodynamic characteristics of the interaction of polymer and solution strongly depend on the charge state of the polymer. The neutral polymer without polar groups on the surface (-OH, $-NH_2$, etc.) is hydrophobic and polymer segments are not solvated by water molecules. This leads to the difficult penetration of solvent molecules into the volume of the polymer film. If the neutrally charged polymer has polar groups in its structure (-OH, $-NH_2$, -COOH, etc.), water molecules will readily enter the polymer and the polymer will contain the water molecules in its volume. This happens because polar groups increase the wettability (and decrease the hydrophobicity) of a polymer film. [35] Ions in the electrolyte penetrate the volume of neutrally charged polymer if their van der Waals and ion-dipole interactions with the polymer are strong. In this case, electrolyte ions can be solvated (hydrated) by both the polymer and the solvent molecules. Moreover, a hydrophobic, nonpolar polymer will interact with hydrophobic ions more strongly. If those were cations, the surface of the polymer would be positively charged, which would be compensated by the excess of negatively charged anions in the solution. The situation is different if the polymer interface is not permeable for one of the ions. In this case, the polymer film works like an ion-exchange membrane. This happens often when the polymer is charged. Despite a large number of articles about the synthesis and the polymerization mechanisms [14,29,36–38], structure [39–42], morphology [43,44], and electrochemical properties of PPy [21,45–47], none of those work investigates relationships between the electrochemical properties of PPy in varying electrolytes, its atomic and electronic structure and synthesis conditions. Our work is dedicated to filling part of this gap. In our study, both influence of a solvent on functional composition, structure and morphology of PPy and influence of these properties on PPy electrochemical behaviour and stability in varying electrolytes were investigated. A study of PPy morphology demonstrates that the solvent used for synthesis affects only the size of PPy's particles while their shape remains identical. At the same time, synthesis conditions define the atomic composition of PPy and valence states of atoms in the polymer chains. Electrochemical properties are determined both by the PPy structure (morphology and atomic composition) and the nature of the electrolyte. All investigated parameters were evaluated in accordance with the strength of their influence on the electrochemical characteristics: Most important is the nature of the electroyte, nitrogen species concentration in the material (aromatic species can participate in redox reactions) and charge of the polymer surface. Prevailing oxygen-containing functional group (OCFGs) which can participate in redox reactions have lower effect. Size of the polymer particles does not influence on electrochemical properties significantly.

2. Experimental section

2.1. Synthesis of PPy samples.

The PPy samples were synthesized by oxidative chemical polymerization using pyrrole monomer as a precursor (Acros organics, reagent grade 98%). $FeCl_3*6H_2O$ (Sigma Aldrich, chemically pure) was chosen as an oxidant. Three different solvents were chosen as polymerizing media: water (distilled), ethanol (Sigma Aldrich, reagent grade > 99.8 %), acetonitrile (Chimmed, reagent grade > 99.8 %). Firstly, the 1M solutions of pyrrole (100 ml) and $FeCl_3$ (100 ml) were prepared in the selected solvent. 1 μl of surfactant (TWEEN-20) was added to the monomer solution to increase the solubility of pyrrole and homogeneity of a precipitated polymer. Secondly, the solution of $FeCl_3$ was added drop by drop to the pyrrole solution (molar rating of monomer/oxidant are equal to 1:1). Dropping the oxidant solution lasted for half an hour with medium stirring. A blue-green precipitate began to be formed in the solution. With the further addition of an oxidizing agent, the polymer changed its color to black. The synthesized polymer was filtered on a polymer filter. Obtained black precipitates were washed with distilled water (100 ml) for removing the remaining Fe^{2+} and Fe^{3+} salts. Then samples were washed with ethanol (50 ml) for removing the remaining solvent. The polymer samples were air-dried for three days. As the result, three different polymer samples were synthesized. The PPy samples obtained in water, ethanol and acetonitrile were labeled as PPyWat, PPyEth, and PPyAN, respectively.

2.2. Characterization methods

The morphology of the samples was studied by SEM and HRTEM using a JEOL JIB 4700F microscope (JEOL Ltd., Japan) with accelerating voltage of 5 keV and JEOL JEM-2200FS (JEOL Ltd., Japan) microscope, respectively. The samples were applied to the holder using carbon tape and placed into the microscope chamber for SEM investigations. Samples were applied on copper meshes using an ultrasonic probe and then copper meshes were applied on the holder and placed into a vacuum microscope chamber. The functional composition of samples was investigated by FTIR, Raman and XPS spectroscopy. FTIR spectra of the samples were obtained using IFS-85 Bruker (Bruker, Ettlingen, Germany) in a spectral range from 400 to cm^{-1} to 2600 cm^{-1}. The samples were pressed in a tablet with KBr (with the material:KBr ratio 1:150 mg). Raman spectra of the samples were obtained using a Horiba Jobin-Yvon LabRAM HR UV-NIR spectrometer (Horiba ltd., France). Spectra were registered using argon laser excitation with wavelength λ = 514.523 nm in the range from 100 to 4000 cm^{-1}. The samples were applied on the glass substrate, the laser beam was focused on a sample with a diameter of spot ~ 0,3 mm. The measured spectra were processed by normalizing. XPS spectra of the samples were measured using the resources of the Russian-German channel of the Berlin center for synchrotron radiation (BESSY, Berlin, Germany). The energy of the storage ring was 30 keV with a current value of ~ 100 mA. The measuring chamber was equipped with a CLAM4 spherical electron energy analyzer. Subtraction of the background and decomposition of the spectra into components were carried out using Casa XPS 2.3.16 software (Casa Software Ltd., Devon, UK). The content of the elements was estimated by the integrated intensity of the C 1s, O 1s, N 1s lines considering the photoionization cross-sections of the elements at given photon energy. All spectra and all lines were taken at three points and averaging. The energy binding and normalization of the spectra were carried out with the OriginPro 2015 software (OriginLab Corp., Northampton, Massachusetts, USA).

2.3. The preparation of electrode films

5-7 mg of the active material was weighed on an analytical balance (AND GR-202). The material was mixed with 3 – 4 drops of ethanol and milled by a pestle in an agate mortar. 1 μl of polyvinylidene difluoride aqueous suspension (64 mass %) (F4D, Russia), used as a binder, was added in the ethanol suspension of the investigated sample and mixed. The obtained mixture was transferred to a glass board and rolled out using a quartz tube. The rolling of the electrode was carried out until the formation of a uniform film, which could be easily separated from the glass surface. The resulting square film (1×1 cm) was air-dried until ethanol evaporated. The obtained films were placed on Pt foil for further electrochemical measurements without additional binding agents.

2.4. Electrochemical measurements

The electrochemical behavior of the PPy samples was studied by the cyclic voltammetry method (CV) with a linear potential scan rate. Measurements were carried out using a three-electrode cell with an Ag|AgCl (filled by 3.5M KCl) reference electrode (ESr-101010, Measuring technologies, Russia). The potential of the Ag|AgCl reference concerning a standard hydrogen electrode is 0.208 V. Platinum foils were used as a current collector for the active material electrode and the counter electrode. The electrochemical cell was connected to a potentiostat-galvanostat P-45X (Electrochemical Instruments, Russia). 1M aqueous solutions of H_2SO_4 (pH ~ 0), NaCl (pH ~ 7) and KOH (pH ~ 14) were used as an electrolyte. The measurements were carried out in a potentiodynamic mode with a 1V potential window at scan rates 2, 5, 10, 20, 50, 100 mV s^{-1}. The ranges [0; 1] V, [0,5; 0,5] V and [-0,9; 0,1] V vs. Ag|AgCl reference electrode were chosen for 1M aqueous solutions of H_2SO_4, NaCl and KOH, respectively. All obtained CV curves were compared with a hysteresis of Pt cell in the same conditions [48,49]. Cell contribution in CV curves is less than 1%. The specific capacities of the materials were calculated according to the eq. 1:

$$C_{Sp} = \frac{\oint I dU}{2 \cdot \Delta U \cdot m} \qquad \text{(eq. 1)}$$

where C_{Sp} is the specific capacity of the material, Fg^{-1}; i is the current, A; du is the differentially small increment of potential, V; ΔU is the range of potentials, V; V_s is the scan rate, mVs^{-1}; m is the mass of the electrode active material, g.

Electrochemical impedance spectroscopy (EIS) was used for the investigation of resistive and diffusion characteristics of the materials. Measurements were carried out in the three-electrode cell described earlier using a potentiostat-galvanostat P-45X (Electrochemical Instruments, Russia). The 1M aqueous solutions of H_2SO_4 (pH ~ 0), NaCl (pH ~ 7) and KOH (pH ~ 14) were used as an electrolyte. The Bias potential, the amplitude of the sinusoidal signal and the frequencies range were equal to 0V, 20 mV and [100 000; 0.5] Hz, respectively for all measurements.

3. Results & discussion

Acetonitrile, ethanol and water solutions of pyrrole monomer as a precursor and 1M $FeCl_3*6H_2O$ as an oxidizing agent were used to investigate the influences of the synthetic medium on electronic structure and morphology of PPy (more detailed information can be found in the Experimental section). Figure 3 demonstrates scanning electron microscopy (SEM) and high-resolution transmission microscopy (HRTEM) images of the PPy samples with different magnifications. The nature of the synthetic medium affects the particle size, while the shape of the particles is identical. Using the aprotic polar solvents (acetonitrile) as a synthetic medium allows obtaining a PPy sample (PPyAN) with the size of particles 0.50 – 0.75 μm (Figure 3b). Using the proton polar solvents (ethanol and water) as the synthetic media allows to synthesize a polymer with the size of 0.10 – 0.25 μm for the sample prepared in ethanol (PPyEth) (Figure 3a) and of 0.75 – 1.00 μm for the sample prepared in water (PPyWat) (Figure 3c). HRTEM investigation of the samples shows that all the samples have an amorphous microstructure, moreover, with an increase in the particle size, the polymer layers form a denser structure. Hence, the nature of the synthetic medium affects only the size of the particles, while the shape and microstructure of the particle remain the same for all the investigated samples. An earlier work [44] devoted to the effect of synthetic conditions on PPy morphology suggests that PPy morphology is directly affected by the dispersion state in the reaction medium. It means that if the oxidizing agent and pyrrole solution have a similar solvent, the polymerization proceeds in the full volume of the reacting mixture and PPy formation is around nucleation centers (around insoluble pyrrole oligomers [25]). This phenomenon has been described in detail for PANI in [50].

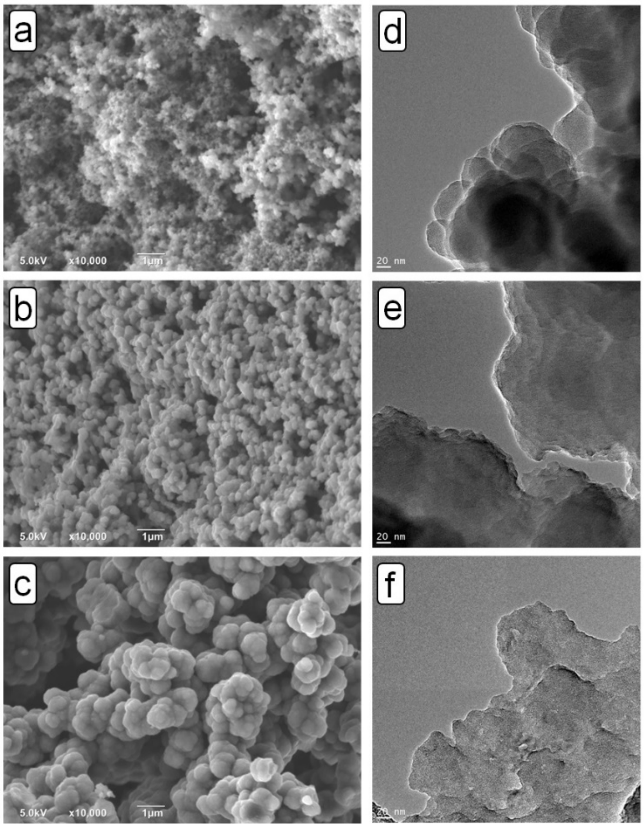

Figure 3. SEM images of the samples (a) PPyEth, (b) PPyAN, (c) PPyWat and HRTEM images of (d) PPyEth, (e) PPyAN and (f) PPyWat.

Analysis of the Fourier-transformed infrared (FTIR) spectra of the PPy samples (Figure 4a) shows that all the samples contain carbonyl functional groups (1872 cm^{-1}). This indicates the occurrence of secondary reactions in the system during the synthesis process. [51] The shifts of the peaks at 1531 – 1548 cm^{-1} and 1285 – 1312 cm^{-1} correspond to valence vibrations of C=C/C=N and C-N bands indicating a different number of rings in the polymer chains [52] (Figure 4b). A shift of these peaks to a smaller value in the spectra of the PPyWat and PPyEth samples indicates a lower ring number in their chain when compared to the PPyAN sample. This also indirectly indicates that the polymer chains terminate while the secondary reactions occur in the ethanol and water synthetic media. The peaks in the range from 1145 to 1178 cm^{-1} are attributed to the N-H, C-H valence vibrations. [53] The peaks in the ranges of 1087 – 1096 cm^{-1}, 1033 – 1047 cm^{-1}, 1000 – 1011 cm^{-1}, 887 – 921 cm^{-1}, 847 – 866 cm^{-1}, 773 – 787 cm^{-1} are ascribed to the deformation vibrations of the nonequivalent C-H bonds. [27] The peaks in the range 964 – 969 cm^{-1} correspond to the 'ring breathing'. These peaks are characteristics for polymers and show that all PPy samples have branched structures with nonequivalent carbon atoms.

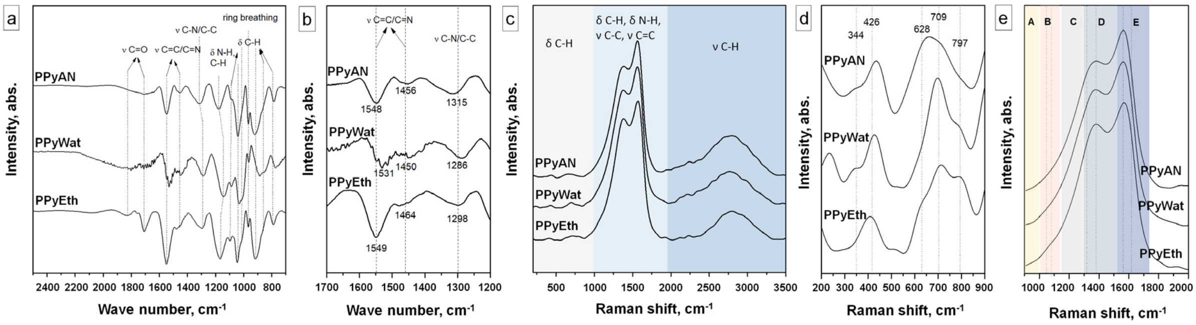

Figure 4. (a) Overall FTIR spectra; (b) the FTIR spectra in range from 1200 to 1700 cm^{-1}; (c) overall Raman spectra of the PPy samples and the Raman spectra in the ranges (d) from 200 to 900 cm^{-1} and (e) from 900 to 2000 cm^{-1}.

The Raman spectra of the samples are divided into three areas (Figure 4c). The first one from 200 to 900 cm^{-1} corresponds to the δ C-H out-of-plane vibrations, the second one consists of peaks related to the δ C-H, δ N-H vibrations and ν C-C and ν C=C, the third one corresponds to the ν C-H vibrations. Five peaks are observed in the first area at 344 cm^{-1}, 426 cm^{-1}, 628 cm^{-1}, 709 cm^{-1} and 797 cm^{-1} (Figure 4d). All these peaks correspond to δ C-H out-of-plane vibrations of non-equivalent C-H bonds of pyrrole rings. [54] The second area is divided into five regions (Figure 4e). The first one from 900 to 1000 cm^{-1} (called A) corresponds to both ring deformation (analog to the "breathing mode" in the FTIR) and δ C-H out-of-plane vibrations [55]. The second region from 1000 to 1150 cm^{-1} (called B) corresponds to δ C-H in-plane vibrations [56] and polaron, bipolaron vibrations. The third region from 1150 to 1300 cm^{-1} (called C) corresponds to δ N-H in-plane vibrations and ring stretching vibrations. The fourth region from 1300 to 1450 cm^{-1} (called D) is responsible for ν C-C bonds in dication, cation and neutrally charged molecules [57]. The last region from 1550 to 1700 cm^{-1} corresponds to ν C=C, ν C=N backbone vibrations in dication, cation and neutrally charged molecules. [58] All the polymers consist of neutrally and positively charged species. Moreover, the width of the peaks in the D and E regions corresponds to cations, dications and neutrally charged species in the samples. The Raman spectra of the samples differ only in the intensity of the D and E regions which correspond to different concentrations of the pyrrole rings in the quinoid and aromatic forms and their different charge states. More information on the ratio of the different carbon and nitrogen species can be obtained from X-ray photoelectron spectroscopy (XPS) data.

Investigation of the functional composition of the polymer samples and surface concentration of the functional groups were performed by the XPS method. The PPy samples were excellently cleared from Fe^{2+} and Fe^{3+} salts because the XPS spectra do not contain peaks related to Fe species (Figure S1a). N:O ratios of the PPy samples depend on the synthetic medium (Figure S1b). The PPyAN sample has the lowest amount of oxygen (~ 10 at. %) and the highest of nitrogen (~ 18 at. %) with N:O ratios ~ 1.8:1. The use of the oxygen-containing solvents as a synthetic medium leads to the increasing of the oxidation degree of the polymer samples: The

PPyWat sample contains ~ 7 at. % of N and 16 at. % of O (N:O ratio ~ 0.44:1), PPyEth contains ~ 10 at. % of N and 15 at. % of O (N:O ratio ~ 0.67:1).

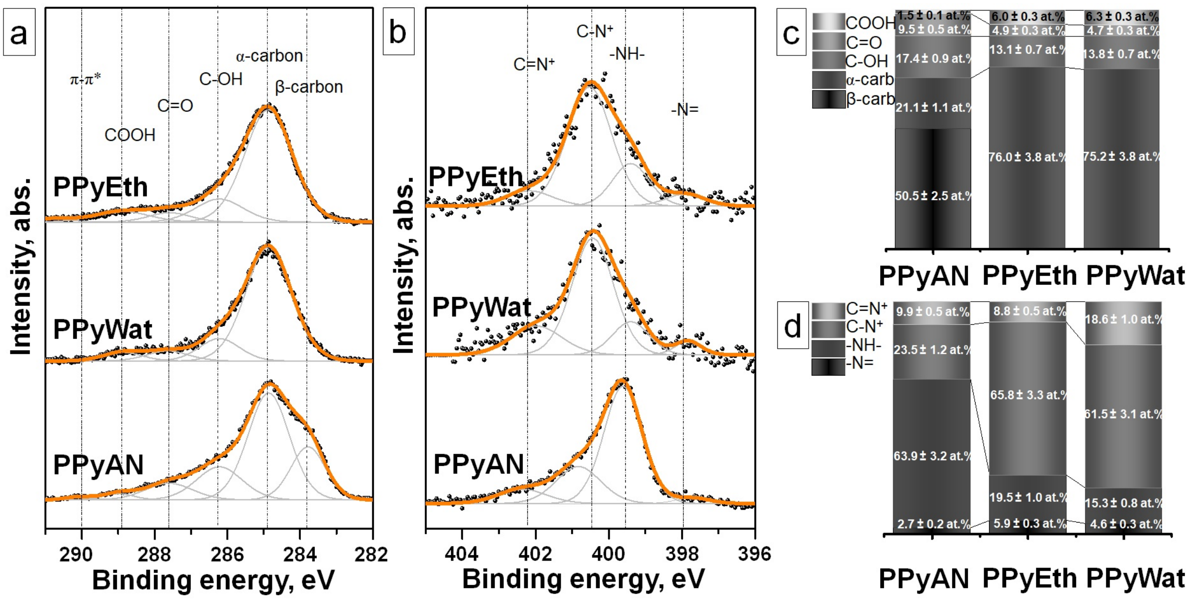

Figure 5. XPS (a) C 1s and (b) N 1s spectra of the PPy samples and atomic concentrations of the different (c) carbon and (d) nitrogen species.

The deconvolution of the C 1s spectra to the six components is shown in Figure 5a. A peak with a binding energy of 283.8 eV corresponds to the formation of C–C bonds at the β-position of the pyrrole ring (see Figure 1) [59]. This peak is explicitly presented only in the PPyAN sample, which allows concluding that only the PPyAN sample has a branched secondary structure (see Figure 1). The next peak with an energy of 284.88 eV corresponds to the formation of a C–C bond at the α-position of the pyrrole ring. [60] The peak with the binding energy 286.26 eV corresponds to C-OH, C=N =C-NH$^+$ (polaron) defects [61]. The peak at 287.60 eV corresponds to C=O and C=N groups [62] and the one at 288.91 eV is ascribed to N-C=O, -COOH –C=N$^+$ (bipolaron) defect formation [62–64]. This fact indicates the occurrence of side reactions during the synthesis with the incorporation of oxygen atoms into the structure and further oxidation/reduction of the corresponding functional groups. [62]

Calculation of the atomic concentrations of individual forms shows that the oxygen-containing functional groups (OCFGs) ratio on the surface of the material depends on the synthetic medium (Figure 5c). For example, in the PPyAN sample, the hydroxyl (~ 18 at.%) and carbonyl groups (~ 9 at.%) prevail, while the content of carboxyl groups is ~ 2 at. %. For the PPyEth sample the ratios of OCFGs are changed. In this sample, the amount of the carboxyl groups increases (~ 6 at.%) while the number of hydroxyl and carbonyl decreases compared to PPyAN (~ 13 at.% and ~ 5 at.%, respectively). The numbers of the carbonyl and carboxyl groups in PPyWat and PPyEth are the same, whereas the number of the hydroxyl (~ 14 at.%) groups strongly decreases compared with PPyAN.

The N 1s XPS spectra of the samples were decomposed to four peaks (Figure 5b). The peaks with binding energy 397.94 and 399.67 eV correspond to the PPy fragments with a neutral nitrogen atom species –N= and –NH–, respectively [62]. The peaks with the binding energy 400.76 eV and 402.39 eV correspond to the $C–N^+$ and $C=N^+$ positively charged nitrogen species called the polaron and bipolaron in literature [62,65]. It is shown that the PPyAN sample predominately consists of the neutral charged species (~ 67 at. %), while PPyWat and PPyEth consist of the charged species (~ 81 at. % and ~ 75 at. %, respectively) (Figure 5d). Moreover, the high value of the –NH– species in PPyAN indicates the presence of a conjugated aromatic system, which indirectly indicates the highest conductivity among the PPyAN sample.

It can be concluded that synthetic medium strongly affects the secondary structure, N:O and C:O ratio and nitrogen and oxygen species. So, the use of a synthetic medium with a low OCFG or water concentration, such as acetonitrile, leads to branched secondary polymer structure formation with α-α’ and α-β’ bonds. The formed polymer has maximal nitrogen concentration and minimal oxygen concentration. Predominantly nitrogen species are neutrally charged, and the polymer has carbonyl and hydroxyl OCFG forms. Change of the synthetic medium nature leads to the differences in the PPy structure. Thus, it is shown for the polyaniline chemical oxidation processes that the presence of the reactive OCFGs in the synthetic medium leads to the incorporation of the OCFGs in the polymer structure [66]. Hence, using the ethanol and water media leads to the formation of the linear secondary structure only with the α-α' bonds (it can relate to the incorporation of the OCFGs in the β-positions of the pyrrole rings), decrease in nitrogen concentration and increase in oxygen concentration. The concentration of the neutrally charged nitrogen species and carbonyl, hydroxyl OCFGs decreases, whereas the concentration of the carboxyl groups increases. Thus, the N:O ratio, carboxyl and hydroxyl OCFGs and positively charged nitrogen species concentration strongly depend on water quantity in the synthetic medium.

Properties / Sample	Particles size	N:O ratio	O:C ratio	Carboxyl groups	Carbonyl groups	Hydroxyl groups	Positively charged nitrogen species ($C=N^+$,$C-N^+$)	Neutrally charged nitrogen species (-NH-, -N=)	Aromatic pyrrole rings	Quinoid pyrrole rings
PPyAN	● ● 0.50 – 0.75 µm	● ● ● 1.8:1	● 0.14:1	● 1.5 ± 0.1 at. %	● ● 9.5 ± 0.5 at. %	● ● ● 17.4 ± 0.9 at. %	● 33.4 ± 1.7 at. %	● ● ● 66.6 ± 3.3 at. %	● ● ● 63.9 ± 3.2 at. %	● 2.7 ± 0.2 at. %
PPyEth	● 0.10 – 0.25 µm	● ● 0.67:1	● ● 0.21:1	● ● 6.0 ± 0.3 at. %	● 4.9 ± 0.3 at. %	● ● 13.1 ± 0.7 at. %	● ● 74.6 ± 3.8 at. %	● ● 25.4 ± 1.3 at. %	● ● 19.5 ± 1 at. %	● ● 5.9 ± 0.3 at. %
PPyWat	● ● ● 0.75 – 1.00 µm	● 0.44:1	● ● 0.20:1	● ● 6.3 ± 0.3 at. %	● 4.7 ± 0.3 at. %	● ● 13.8 ± 0.7 at. %	● ● ● 80.1 ± 4.1 at. %	● 19.9 ± 1.1 at. %	● 15.3 ± 0.8 at. %	● ● 4.6 ± 0.3 at. %

Figure 6. Significance of the investigated structural parameters for the studied samples. One dot in the table cell means that the parameter value for this sample is the smallest among all samples while three dots mean that the parameter value for this sample is the highest.

Summarized comparison of the sample properties is represented in Figure 6. The functional group composition, particle size and structure of the polymer chain strongly depend on the synthetic medium. Using acetonitrile as a synthesis medium allows to synthesize a material with medium particle size, branched secondary structure (with α-α' and α-β' bonds), the highest concentration of nitrogen and lowest concentration of oxygen. Moreover, most of the nitrogen atoms in this sample are in the uncharged state and correspond to nitrogen in the pyrrole aromatic units, which indicates the lowest positive surface charge among all the samples. Predominantly the hydroxyl and carbonyl OCFGs are formed on the surface of the material. When acetonitrile is replaced by ethanol, particle size and nitrogen concentration decrease, oxygen concentration increases, and the secondary polymer structure is represented only by α-α' bonded units. In this case, predominantly hydroxyl groups are formed. The concentration of the charged nitrogen species increases ~ 2.2 times and the concentration of the aromatic pyrrole rings decreases ~ 3.4 times. Using water as the synthetic medium allows to synthesize a material with the highest particle size, lowest nitrogen concentration and secondary polymer structure represented only by α-α' bonded units. In this sample concentration of the carbonyl and carboxyl groups are the same as for the PPyEth sample and the concentration of the hydroxyl groups is close to that of PPyWEth, the highest concentration of the positively charged nitrogen species is obtained.

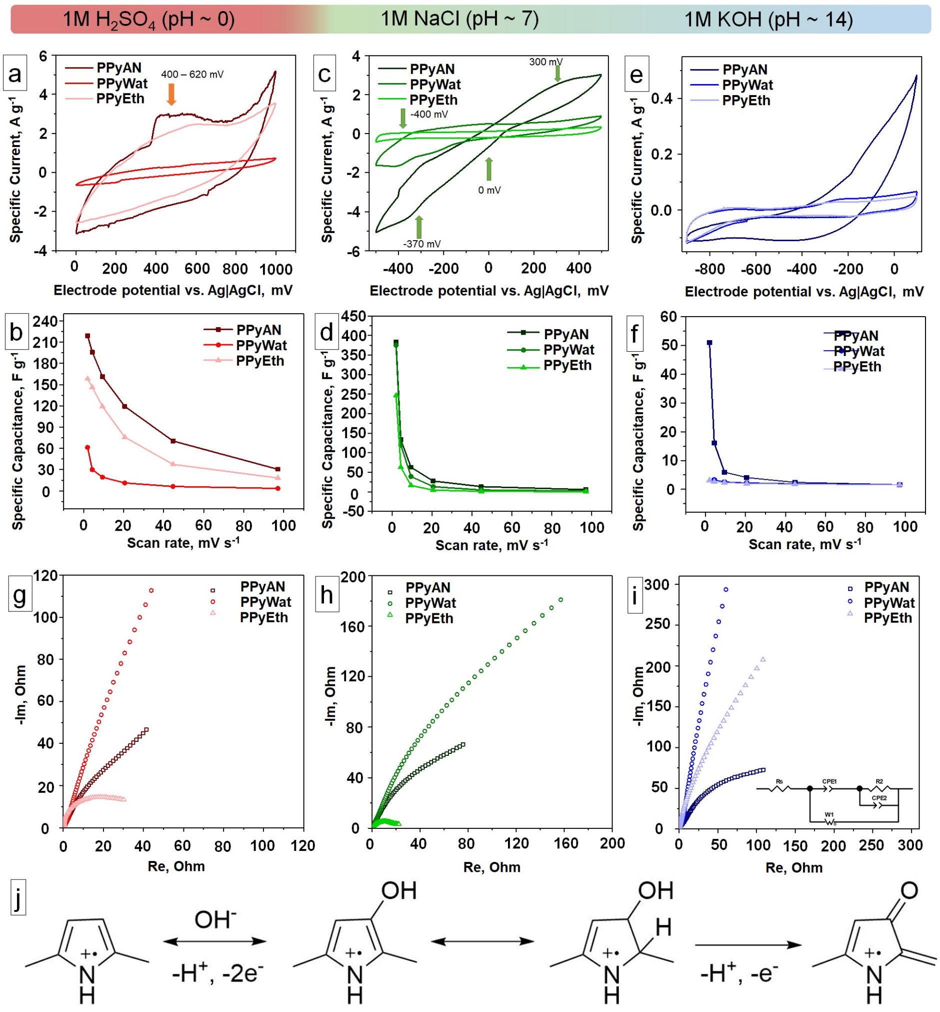

Figure 7. CV curves at the scan rate of 10 mV s^{-1} and specific capacitance of the PPy samples in 1M aqueous electrolytes of (a,b) H_2SO_4; (c,d) NaCl and (e,f) KOH; EIS spectra of the samples in (g) 1M H_2SO_4, (h) 1M NaCl, (i) 1M KOH. (Fitted spectra see in Figure S4) and (j) oxidation process of the pyrrole unit.

The electrochemical properties of the samples were studied by cyclic voltammetry (CV) with a linear potential scan mode (Figure S2). Aqueous electrolytes of 1M H_2SO_4 (pH ~ 0), 1M NaCl (pH ~ 7), 1M KOH (pH ~ 14) were chosen as electrolytes. Figure 9 demonstrates CV curves obtained at a potential scan rate of 10 mV s^{-1}.

Since the obtained samples contain both OCFGs and pyrrole rings, it is worth considering which redox reactions can occur in the system. The first is the quasi-reversible oxidation/reduction of OCFGs [67]. In the literature [68,69], these reactions are often given in the following form (eq.2 – eq. 4):

$$> C - OH \leftrightarrow > C = O + H^{+} + e^{-} \qquad \text{(eq. 2)}$$

$$-COOH \leftrightarrow -COO^{-} + H^{+} \qquad \text{(eq. 3)}$$

$$> C = O + e^{-} \leftrightarrow > C - O^{-} \qquad \text{(eq. 4)}$$

In our previous works [67,70] the standard potentials of one of these reactions were determined using a thermally reduced graphite oxide with a controllable amount of OCFGs. It was shown that the oxidation reaction of C-O$^-$ to C=O (eq. 4) proceeds at the potential value 0.369 V vs. Ag|AgCl (3.5 KCl solution) when sweeping towards more positive potentials, the reduction process of C=O to C-O$^-$ (eq. 4) proceeds at 0.552 V when scanning in the opposite direction. Process of C=O oxidation with the formation of –COOH at 0.731 V is observed when sweeping towards more positive potentials, the reduction process from COOH to C=O at 0.306 V is observed when scanning in the opposite direction. These reactions can be determined in the CV curve only when the total amount of OCFGs is less than 13%. If the total amount of OCFGs more, the small difference between the reduction potentials leads to their overlapping on the CV curve and the formation of one intensive broad peak.

During the electrochemical cycling, the incorporation of additional OCFGs and additional oxidation of already presented OCFGs can occur (Figure 7j), similarly to processes on the surface of carbon materials [71] (eq. 5):

$$> -C - H \xrightarrow{[O]} -C - OH \xrightarrow{[O]} > C = O \xrightarrow{[O]} -COOH \xrightarrow{[O]} CO_2 \qquad \text{(eq. 5)}$$

The CV curves of the materials measured in 1M H_2SO_4 have a hysteresis of various shapes and sizes of redox peaks (Figure 7a). Thus, the sample capacities are determined by the occurrence of redox reactions on the polymer surface (pseudo-capacitance) and the transport of the electrolyte ions into its volume (diffusion capacities). PPyEth and PPyAN have a similar hysteresis with one broad oxidation peak at 400 – 620 mV on the anodic scan (potentials converted vs. RHE represented in Table S2.), which corresponds to an irreversible oxidation process on the polymer surface (Figure S2a,d,g). That peak is a merge of several peaks corresponding to the OCFG redox reactions [72] (Figure 7j, eq.2-5) and pyrrole (Figure 2) redox reactions. Analysis of reactions processes character was carried out using Randles-Sevcik equation (eq. 6) and the equation of the contribution the capacitive and insertion processes current in the total peak current at the given potential (eq. 7):

$$I_p = 0.4463 \cdot v^{1/2} \cdot \frac{n^{3/2} \cdot F^{3/2}}{R^{1/2} \cdot T^{1/2}} \cdot C_0 \cdot D_{av}^{1/2} \qquad \text{(eq. 6)}$$

where v is the linear potential scan rate, V s^{-1}; n is the number of electrons involved in the electrochemical process; F is the Faraday constant, 96 ,485 C mol^{-1}; R is the universal gas constant, 8.314 J mol^{-1} K^{-1}; T is the temperature, K; D_{av} is the averaged chemical diffusion coefficient, cm^2 s^{-1}; C_0 is the cation initial bulk concentration (for the anodic potential scanning) or anion concentration (for the cathodic potential scanning) mol cm^{-3}. [73]

$$i(V) = a_1 v + a_2 v^{1/2} \qquad \text{(eq. 7)}$$

where $a_1 v$ and $a_2 v^{1/2}$ are the contribution in the total current at given potential value from the capacitive (redox pseudo-capacitance) and diffusion-controlled (diffusion layer formation) processes [74–76]. It should be noted that if dependencies of current on v are linear – it is ideal EDLC, then the deviation from linearity is conditioned by pseudo-capacitive processes.

Graphs of peak current (I_p) vs. scan rate (v) and the square root of scan rate ($v^{0.5}$) were plotted (Figure S3) for analysis of peak behavior using Randles-Sevick equation (eq. 6) and kinetics characters of the reactions. The linear dependencies of the peak current vs. root square of scan rate ($v^{0.5}$) (Figure S3b) corresponds to the fact that the processes are controlled by diffusion from 2 to 100 mV s^{-1}. This fact also was shown in our previous work devoted to the investigation of composites based on PPy and MWCNT buckypaper. [52] In terms of kinetic dependencies, the linear dependencies of I_p vs $v^{0.5}$ in this region indicate an ideal pseudo-capacitive character of those reactions. The analysis of I_p vs. v shows the linear dependencies only in the range from 2 to 20 mV s^{-1}, which corresponds to a contribution from diffusion layer capacitance and pseudo-capacitive processes. Another way to understand the character of processes is an analysis of the CV data at various sweep rates using equations (eq. 8-9) [77,78]:

$$i = a \cdot v^b \qquad \text{(eq. 8)}$$

$$\log(i) = \log(a) + b \cdot \log(v) \qquad \text{(eq. 9)}$$

where the measured current i obeys a power law relationship with the scan rate. Both a and b are adjustable parameters. The b parameter can be calculated as the slope of dependencies log(i) vs. log(v). So, when b is close to 1, the current has a predominantly capacitive nature. If b is equal to 0.5, the current flow at all potentials has linear dependencies on the square root of the sweep rate, which means it is an ideal diffusion-controlled process. As it is shown in Figure S2, all samples have a different value of the b parameter. Thus, PPyAN has a predominantly capacitive nature. The PPyEth sample shows intermediate behavior, PPyWat has predominantly diffusion-controlled behavior. Hence, it can be concluded that the nature of the processes differs for different samples. PPyAN shows predominantly capacitive behavior, PPyEth has intermediate behavior and PPyWat has diffusion-controlled behavior. This peak has the highest intensity on the CV curve of the PPyAN sample due to the high concentration of the aromatic pyrrole units (64 at. %) which are oxidized with the formation of the quinoid pyrrole units, polaron particles, hydroxyl OCFGs (18 at. %) and carbonyl groups [72] (Figure 7j, eq.2). This peak is depressed on the CV curve of the PPyEth sample due to the low concentration of the aromatic pyrrole units (19 at. %) and mainly determined by oxidation of the hydroxyl groups. The specific capacities of the samples reach 160 and 230 F g^{-1} in 1M H_2SO_4 at scan rate 5 mV s^{-1} for PPyEth and PPyAN, respectively (Figure 7b) whereas specific capacitance of PPyWat reaches only 60 F g^{-1} in the same conditions. Such a large difference in the values of the specific capacities of the materials is explained by the different surface charges of the samples. As is noted above in the Introduction part, high surface charge leads to the creation of an excessive concentration of anions on the material surface and the repulsion of cations, which creates a dense diffusion layer mainly on the surface of the material preventing penetration of electrolyte ions into the bulk of an electrode material. The sizes of the solvated SO_4^{2-} anions (3.79 Å) are much larger than the size of H^+ (2.80 Å) which leads to obstruction of cations diffusion into the volume of the material and to a decrease in the hysteresis size. Since the concentration of the positively charged nitrogen species increases in order PPyAN (34 at. %) < PPyEth (75 at. %) < PPyWat (81 at. %) and drop of the specific capacitance occurs in the same order PPyAN (230 F g^{-1}) > PPyEth (160 F g^{-1}) > PPyWat (60 F g^{-1}), the nitrogen species mainly affect the specific capacitance in 1M H_2SO_4 due to their influence on the polymer surface charge and participation in electrochemical reactions (Figure 2). Hence, if the polymer predominantly contains neutrally charged nitrogen atoms in the pyrrole units, the reaction of their oxidation with the formation of the pyrrole units in the quinoid form and polaron particle occurs. After that, additional oxidation of the PPy chain can proceed with the formation of the bipolaron particles. This means that the specific capacitance of the samples with a high concentration of the pyrrole rings in the aromatic form and neutrally charged nitrogen are boosted by the process of PPy chain oxidation with the formation of the polaron and bipolaron particles. Such parameters as particle and pore size and OCFG quantity have a secondary influence. The deviation from linearity between increasing positively charged nitrogen atom concentration and decreasing specific capacitance of the samples occurs due to the difference between the polymer primary structures and the influence of additional parameters such as the particle and pore size and OCFG quantity.

CV curves of the materials measured in 1M NaCl aqueous electrolyte are represented in Figure 7c. The behaviour is different in 1M NaCl electrolyte (Figure S2b,e,h): All the materials have different hysteresis shapes. The PPyAN sample has broad symmetrical hysteresis with low-intensity peaks at -350 mV, 300 mV when sweeping towards more positive potentials and at -370 mV when scanning in the opposite direction (potentials converted vs. RHE represented in Table S2). Peaks at 300 mV in the sweep going to positive potentials and -370 mV on the sweep towards negative potentials are represented by oxidation and reduction of hydroxyl and carbonyl OCFGs, while the peak at -350 mV corresponds to oxidation of carboxyl OCFGs. The PPyWat and PPyEth samples have similar asymmetric hysteresis forms with one broad peak from -400 mV to 0 mV when sweeping towards higher positive potentials and one broad peak from -100 mV to -400 mV when scanning in the opposite direction. Asymmetry in the shape of the curves is featured by wide peaks indicating carboxyl groups oxidation and reduction. As written earlier, the potentials of all reactions are recalculated vs. RHE (see Table S2) for their easier comparison in a different medium. It is shown that predominantly potentials are close to each other. Shifts of the potential values in 1M NaCl occur due inertness of nitrogen atoms. In 1M H_2SO_4 all peaks merge into one and shift due participation of nitrogen atoms in electrochemical reactions. The specific capacitance values decrease in order PPyAN (385 F g^{-1}) ~ PPyWat (377 F g^{-1}) > PPyEth (250 F g^{-1}) in the same manner as the change of particle size PPyWat (0.75 – 1.00 μm) ~ PPyAN (0.50 – 0.75 μm) > (0.10 – 0.25 μm). This behaviour is attributed to the electrolyte ion size, Na^+ and Cl^- have the ionic (0.95 and 1.81 Å, respectively) and close solvated radius values (3.58 and 3.32 Å, respectively) and value of charge (Table S1) [79], which leads only to partial blocking of cation penetration by an excess concentration of adsorbed anions (chemisorbed) on the surface of the material. This fact leads to a weakening of the effect of the surface charge on the specific capacitance of the materials. Particle size has the main influence on the specific capacitance of the samples in 1M NaCl. Nitrogen species have a secondary influence on the specific capacitance in 1M NaCl because they do not participate in redox reactions.

CV curves of the materials measured in 1M KOH aqueous electrolytes are represented in Figure 7e (Figure S2c,f,i). The PPyWat and PPyEth samples have hysteresis corresponding to a flat cell with platinum electrodes. [49] The PPyAN sample has asymmetric hysteresis which corresponds to structural changes in the polymer as rearrangement of the aromatic pyrrole units to quinoid (Figure 2a). The specific capacitance of the samples changes in order PPyAN (50 F g^{-1}) > PPyEth (3 F g^{-1}) ~ PPyWat (3 F g^{-1}). The same order is observed in the concentration of the aromatic pyrrole units in the samples PPyAN (64 at. %) > PPyEth (19 at. %) ~ PPyWat (15 at. %). In the case of the electrolyte, the situation is similar to 1M NaCl, which suggests that surface charge does not affect the specific capacitance, but the quality of the aromatic pyrrole units affects due to their participation in the electrochemical reaction. The redox activity of the PPy samples is different in the different electrolytes due to different redox processes, in 1M H_2SO_4 oxidation of both pyrrole units and OCFG occurs, unlike in 1M NaCl where solely reversible redox processes of OCFG is observed. The main reason why the effectiveness of the PPy samples in the 1M KOH electrolyte is lower than in the others is the gradual diminishment of π – conjugated system length due to their oxidation process (Figure 7j). It can be concluded that influences of the electrolyte and material properties decrease in order: electrolyte parameters (a charge, size and nature of ions) > nitrogen species and OCFGs > size of particles and pores.

In addition to the CV data, EIS spectra for all the materials were recorded to study the processes of charge transfer and resistive properties of the materials. Obtained data were analyzed using an equivalent circuit [80] represented in Figure 7i. (insertion). In that scheme

R_s is the contact and electrolyte resistance, CPE_1 is the diffusion capacity of the polymer films (analog of the electric double layer capacitance for the carbon materials), R_2 and CPE_2 are the charge transfer resistance and redox capacity of the polymer film which is afflicted to the amount of redox-active sites, respectively. The W_o element corresponds diffusion of the electrolyte ions [80]. It is shown that good convergence of the experimental and fitted spectra is achieved using this model. The fitting parameters are represented in the Supporting Information (see Table S2).

Values of R_s are in the range from 0.09 to 0.44 Ω for all samples and all electrolytes that correspond to low contact resistance at the current collector/polymer film interface [81,82]. Contact resistance value depends on both the material and electrolyte nature. The shape and size of the material particles and changes in the polymer conductivity during electrolyte ions penetration influence the contact resistance. Consequently, with the increasing particle size, the contact resistance increases as well. As noted earlier, the CPE_1 element corresponds to the diffusion capacitance of the samples and it is represented by a depressed semi-circle in the high-frequencies region. It should be noted that diffusion layers in polymers are in near-surface layers of polymer and on their surface. Hence, the thickness of the diffusion layer varies depending on such polymer properties as surface charge, morphology, functionalization, etc. The CPE_1-P parameter which corresponds to the homogeneity of the diffusion layer of the samples varies from 0.82 to 0.88 depending on the sample and electrolyte and means that CPE_1-T parameter measures in F (Farad). The higher the value of the CPE_1-P parameter, the more ideal, i.e. less porous and more homogeneous, the polymer layer is. It is clearly shown that the diffusion capacitance of the samples does not depend on its homogeneity but has the same dependencies as the specific capacitance of the samples on the surface charge of the materials. The size of the depressed semi-circle decreases in order PPyWat > PPyAN > PPy Eth for the samples in 1M H_2SO_4 and 1M NaCl and in order PPyWat > PPyEth > PPyAN in 1M KOH

(Figure S4). R_2 is the charge transfer resistance for the polymer electrochemical reactions and these values are in the range from 0.11 Ω to 6.59 Ω depending on the material and electrolyte nature. Moreover, the charge transfer resistance strongly depends on the nature of the electrolyte and increases in order 1M H_2SO_4 < 1M NaCl < 1M KOH. CPE_2 element corresponds to the redox capacity of the electrode materials and the CPE_2-P value varies from 0.82 to 1.00 depending on the sample and electrolyte signifying that the CPE_2-T parameter measures in F (Farad). The size of this depressed semi-circle decrease in order PPyEth > PPyAN > PPyWat for the samples in 1M H_2SO_4 and 1M NaCl and order PPyAN > PPyEth > PPyWat in 1M KOH. W_o element consists of three parameters W_o-R, W_o-P and W_o-T. W_o-P parameter corresponds to the slope of the line, W_o-R – electrolyte resistance and $W_o\text{-}T = L^2/D$ (T_w) (where L – effective diffusion layer thickness and D – effective diffusion coefficient) correspond to the inverted effective diffusion coefficient. *Wo-P* varies from 0.03 to 0.15 and corresponds to a good electrolyte transport, which is confirmed by the low-value range of the W_o-R parameter [0.01;2.51] Ω. *Wo-T* value varies from 10^{-16} to 10^{-20} s indicating a good diffusion, but it should be noted that the diffusion is limited by the effective diffusion thickness that is the same as diffusion layer thickness.

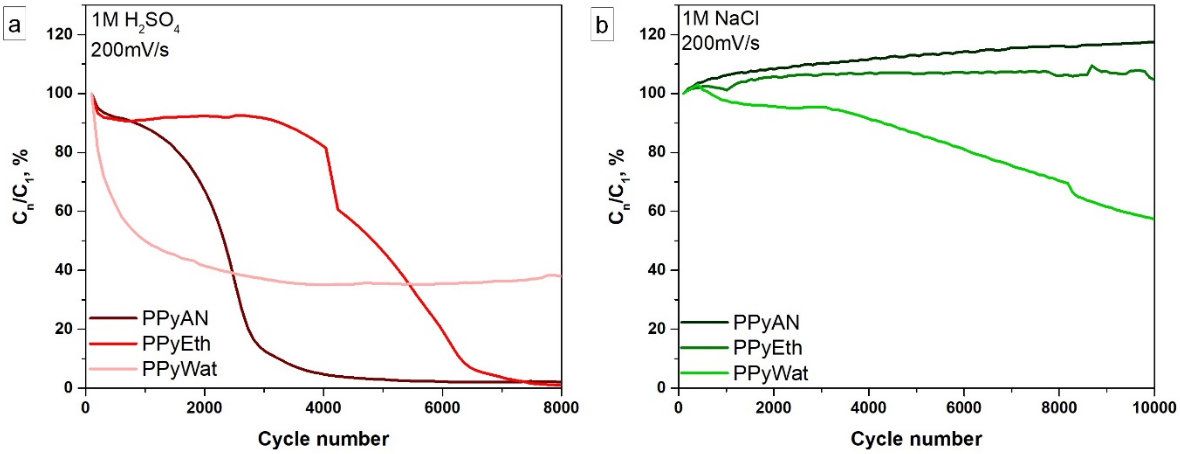

Figure 8. The capacity retention of the PPy samples in 1M aqueous electrolyte of (a) H_2SO_4 and (b) NaCl.

For cycling stability experiments 1M H_2SO_4 and 1M NaCl electrolytes were chosen due to the high capacity of the PPy samples in these solutions. It is shown that the stability of the PPy samples during long cycling is different for the materials with the different electronic structure and electrolyte nature (Figure 8). 1M H_2SO_4 affects negatively the stability of all the PPy films (CV curves are represented in Figure S5a,c,e). PPyAN has the worst stability and its specific capacitance slowly drops to 80% of initial capacity during 2,000 cycles followed by fast drops to 10% (3,000 cycles). The specific capacitance of the PPyWat sample drops fast during the first 3,000 cycles (to 40%) and then stabilizes. The PPyEth sample has a stable specific capacitance over 3,500 cycles and after that degrades fast during 4,500 cycles. The low stability of the PPy samples in the acidic medium can be explained by the low stability of the pyrrole rings in the acidic medium and their oxidation with the formation OCFGs (Figure 7j). The stability of the polymer chains is higher than that of the pyrrole monomers in the solution due to the presence of bonds in chemically active α-position of the rings, which stabilizes the polymer structure in comparison to monomer and prevents oxidation of carbon in α-position. However, reactions of the electrolyte species with the polymer chains can occur when potential is applied. Enhanced stability of PPy in the acidic medium can be reached by the production of composite materials with carbon nanostructures [83] or additional electroactive components [8,84]. The studied samples have the highest stability in the 1M NaCl medium, despite the data obtained earlier [72], where PPy samples have shown better stability in an acidic medium than in neutral. In that study, the PPy samples were obtained by an electrochemical polymerization method and hence, another charge state and particle of the size of PPy was achieved as the samples contained electrolyte species before long cycling. Therefore, in our study opposite results are related to the different charge states, the structure of the polymer films and the absence of other electrolyte species in the polymer before long cycling. The absence of the electrolyte species in the PPy samples before cycling leads to gradual penetration of the electrolyte ions into a volume of the polymer film which explains the increase in specific capacitance for PPyAN and PPyEth between 4,000 and 8,000 cycles and their further stabilization (CV curves are represented in Figure S5b,d,f). The specific capacitance of the PPyWat sample drops during first 3,500 cycles to 95%, then slope of the curve changes and the specific capacitance drops faster to 75% at 8,000 cycle. Hence, the specific capacitance of this sample drops to 60% by 10,000 cycles. All samples have better electrochemical characteristics in the NaCl medium due to the optimal relation between the diffusion layer and electrolyte ions nature and absence of irreversible redox reactions.

It was shown that the solvent used for the synthesis of polypyrrole affects only the size of the PPy particles when its shape remains identical. The atomic composition of PPy and valence states of atoms are affected by the synthetic medium. Electrochemical properties are affected by the PPy structure (morphology and atomic composition) and the nature of the electrolyte. For the first time in our work all investigated parameters were evaluated following the strength of their influence on the electrochemical characteristics. The nature of the electrolyte, the nitrogen species concentration in the material (aromatic species can participate in redox reactions) and the charge of the polymer surface have the most important role than prevailing OCFGs have a secondary effect. The size of the polymer particles does not influence electrochemical properties significantly.

4. Conclusions

It was found that the choice of the solvent for the synthesis of PPy significantly affects the particle size, N:O and O:C atomic ratio, nitrogen species and prevail OCFGs, while the shape of the particles is identical. The particle size depends on the nature of the synthetic medium. Thus, the particle sizes increase in order PPyEth (0.25 – 0.50 μm) < PPyAN (0.50 – 0.75 μm) < PPyWat (0.75 – 1 μm) for the samples obtained in the ethanol, acetonitrile, and water solvents, respectively. Using an oxygen-containing synthetic medium leads to increasing of the C:O ratio, the concentration of the positively charged nitrogen species and the formation of the carboxyl OCFGs and decreasing N:O ratios and hydroxyl OCFGs. Measurements of electrochemical characteristics show that the sample PPyAN has the highest specific capacitance in all electrolytes at 5 mV s^{-1} and its specific capacitance increases in order 1M KOH (50 F g^{-1}) < 1M H_2SO_4 (230 F g^{-1}) < 1M NaCl (385 F g^{-1}). Electrochemical properties of the materials are affected by electrolyte and material parameters in order: nature of the electrolyte (charge and size of ions) ~ nitrogen species concentration in the material (aromatic species can participate in redox reactions) and charge of the polymer surface > prevail OCFGs (can participate in redox reactions) > size of the polymer particles. All the samples have low contact and charge transfer resistance, diffusion capacitance values are higher compared with redox capacitance (some samples have equal values). Diffusion and redox capacitance values do not depend on the homogeneity of the system but depend on the surface charge of the PPy films, nitrogen, and oxygen species. All the samples have similar diffusion characteristics. Stability of the PPy samples increases in order 1M H_2SO_4 < 1M NaCl which is related to the irreversible character of redox processes in the 1M H_2SO_4 electrolyte. Increasing the specific capacitance of the samples during long cycling in 1M NaCl is related to the gradual penetration of the electrolyte species into the volume of the polymer film. Thus, the PPyAN and PPyEth samples have the highest stability during 10,000 cycles in 1M NaCl and can reach specific capacitance more than 385 F g^{-1} and 250 F g^{-1} during 10,000 cycles, respectively. The impedance spectra of the samples correlate with the particle size and surface charge (nitrogen and oxygen species) in the 1M H_2SO_4 and NaCl electrolytes. For 1M KOH, it depends on the nitrogen species as well as in the CV method.

CRediT authorship contribution statement

Iurchenkova A. A. – conceptualizations, methodology, formal analysis, investigation, writing – original draft, visualization; Kallio T. – resources, writing – editing; Fedorovskaya E. O. – formal analysis, resources, supervising, writing– review and editing. All authors have approved the final version of the manuscript.

Declaration of competing interest

The authors declare that they have no known competing financial interests or personal relationships that could have appeared to influence the work reported in this paper.

Acknowledgments

This work was supported by the Ministry of Science and Higher Education of the Russian Federation project No FSUS-2020-0036. We thank HZB (Helmholtz Zentrum Berlin) for the allocation of synchrotron radiation beam time. The TEM was performed on the equipment of CKP “VTAN” in the ATRC department of NSU by G. K. Krivyakin. The authors acknowledge S. A. Martynova for FTIR measurements and E. V. Lobiak for XPS spectra. The SEM was performed on the equipment of Aalto OtaNano Nanomicroscope Center. The Raman spectra were performed on equipment of Aalto OtaNano Low-Temperature Laboratory.

References

[1] A. González, E. Goikolea, J.A. Barrena, R. Mysyk, Review on supercapacitors: Technologies and materials, Renew. Sustain. Energy Rev. 58 (2016) 1189–1206. https://doi.org/10.1016/j.rser.2015.12.249.

[2] X. Wang, X. Lu, B. Liu, D. Chen, Y. Tong, G. Shen, Flexible energy-storage devices: Design consideration and recent progress, Adv. Mater. 26 (2014) 4763–4782. https://doi.org/10.1002/adma.201400910.

[3] P. Simon, Y. Gogotsi, P. Simon, Materials for electrochemical capacitors, Nat. Mater. 7 (2008) 845–854.

[4] L. Dong, C. Xu, Y. Li, Z.H. Huang, F. Kang, Q.H. Yang, X. Zhao, Flexible electrodes and supercapacitors for wearable energy storage: A review by category, J. Mater. Chem. A. 4 (2016) 4659–4685. https://doi.org/10.1039/c5ta10582j.

[5] R. Dubey, V. Guruviah, Review of carbon-based electrode materials for supercapacitor energy storage, Ionics (Kiel). 25 (2019) 1419–1445. https://doi.org/10.1007/s11581-019-02874-0.

[6] L.G. Bulusheva, V.A. Tur, E.O. Fedorovskaya, I.P. Asanov, D. Pontiroli, M. Riccò, A. V. Okotrub, Structure and supercapacitor performance of graphene materials obtained from brominated and fluorinated graphites, Carbon N. Y. 78 (2014) 137–146. https://doi.org/10.1016/j.carbon.2014.06.061.

[7] E.O. Fedorovskaya, L.G. Bulusheva, A.G. Kurenya, Effect of Oxidative Treatment on the Electrochemical Properties of Aligned Multi-Walled Carbon Nanotubes, 52 (2016) 441–448. https://doi.org/10.1134/S1023193516050049.

[8] M.A.A. Mohd Abdah, N.H.N. Azman, S. Kulandaivalu, Y. Sulaiman, Review of the use of transition-metal-oxide and conducting polymer-based fibres for high-performance supercapacitors, Mater. Des. 186 (2020) 108199. https://doi.org/https://doi.org/10.1016/j.matdes.2019.108199.

[9] A.A. Iurchenkova, E.O. Fedorovskaya, P.E. Matochkin, S.Z. Sakhapov, D. V. Smovzh, Supercapacitor behavior of carbon-manganese oxides nanocomposites synthesized by carbon arc, Int. J. Energy Res. 44 (2020) 10754–10767. https://doi.org/10.1002/er.5721.

[10] M. Hu, H. Zhang, T. Hu, B. Fan, X. Wang, Z. Li, Emerging 2D MXenes for supercapacitors: status, challenges and prospects, Chem. Soc. Rev. 49 (2020) 6666. https://doi.org/10.1039/d0cs00175a.

[11] Y. Han, L. Dai, Conducting Polymers for Flexible Supercapacitors, Macromol. Chem. Phys. 220 (2019) 1–14. https://doi.org/10.1002/macp.201800355.

[12] K.S. Ryu, X. Wu, Y.G. Lee, S.H. Chang, Electrochemical capacitor composed of doped polyaniline and polymer electrolyte membrane, J. Appl. Polym. Sci. 89 (2003) 1300–1304. https://doi.org/10.1002/app.12242.

[13] T.F. Otero, J.G. Martinez, J. Arias-Pardilla, Biomimetic electrochemistry from conducting polymers. A review: Artificial muscles, smart membranes, smart drug delivery and computer/neuron interfaces, Electrochim. Acta. 84 (2012) 112–128. https://doi.org/10.1016/j.electacta.2012.03.097.

[14] P. Sengodu, A.D. Deshmukh, Conducting polymers and their inorganic composites for advanced Li-ion batteries: A review, RSC Adv. 5 (2015) 42109–42130. https://doi.org/10.1039/c4ra17254j.

[15] O. Bubnova, M. Berggren, X. Crispin, Tuning the thermoelectric properties of conducting polymers in an electrochemical transistor, J. Am. Chem. Soc. 134 (2012) 16456–16459. https://doi.org/10.1021/ja305188r.

[16] W.H. Kim, A.J. Mäkinen, N. Nikolov, R. Shashidhar, H. Kim, Z.H. Kafafi, Molecular organic light-emitting diodes using highly conducting polymers as anodes, Appl. Phys. Lett. 80 (2002) 3844–3846. https://doi.org/10.1063/1.1480100.

[17] K. Dutta, P.P. Kundu, A review on aromatic conducting polymers-based catalyst supporting matrices for application in microbial fuel cells, Polym. Rev. 54 (2014) 401–435. https://doi.org/10.1080/15583724.2014.881372.

[18] C.R. Martin, Nanomaterials : A Membrane-Based Synthetic Approach, 266 (1994).

[19] G.B. Street, S.E. Lindsey, A.I. Nazzal, K.J. Wynne, The Structure and Mechanical Properties of Polypyrrole, Mol. Cryst. Liq. Cryst. 118 (1985) 137–148. https://doi.org/10.1080/00268948508076201.

[20] R. Balint, N.J. Cassidy, S.H. Cartmell, Conductive polymers: Towards a smart biomaterial for tissue engineering, Acta Biomater. 10 (2014) 2341–2353. https://doi.org/10.1016/j.actbio.2014.02.015.

[21] Y. Huang, H. Li, Z. Wang, M. Zhu, Z. Pei, Q. Xue, Y. Huang, C. Zhi, Nanostructured Polypyrrole as a flexible electrode material of supercapacitor, Nano Energy. 22 (2016) 422–438. https://doi.org/10.1016/j.nanoen.2016.02.047.

[22] J.L. Bredas, G.B. Street, Polarons, Bipolarons, and Solitons in Conducting Polymers, Acc. Chem. Res. 18 (1985) 309–315. https://doi.org/10.1021/ar00118a005.

[23] A.O. Patil, A.J. Heeger, F. Wudl, Optical Properties of Conducting Polymers, Chem. Rev. 88 (1988) 183–200. https://doi.org/10.1021/cr00083a009.

[24] T.H. Le, Y. Kim, H. Yoon, Electrical and electrochemical properties of conducting polymers, Polymers (Basel). 9 (2017). https://doi.org/10.3390/polym9040150.

[25] J. Stejskal, M. Trchová, Conducting polypyrrole nanotubes: a review, Springer International Publishing, 2018. https://doi.org/10.1007/s11696-018-0394-x.

[26] M. Can, H. Özaslan, Ö. Işildak, N.Ö. Pekmez, A. Yildiz, Investigation of catalytic effects of the proton and Lewis acids on oligomerization and chemical polymerization of pyrrole, Polymer (Guildf). 45 (2004) 7011–7016. https://doi.org/10.1016/j.polymer.2004.08.003.

[27] T.H. Chao, J. March, A study of polypyrrole synthesized with oxidative transition metal ions, J. Polym. Sci. Part A Polym. Chem. 26 (1988) 743–753. https://doi.org/10.1002/pola.1988.080260306.

[28] C. Saravanan, R.C. Shekhar, S. Palaniappan, Synthesis of polypyrrole using benzoyl peroxide as a novel oxidizing agent, Macromol. Chem. Phys. 207 (2006) 342–348. https://doi.org/10.1002/macp.200500376.

[29] Y. Tan, K. Ghandi, Kinetics and mechanism of pyrrole chemical polymerization, Synth. Met. 175 (2013) 183–191. https://doi.org/10.1016/j.synthmet.2013.05.014.

[30] D. Brezoi, Polypyrrole films prepared by chemical oxidation of polypyrrole in aqueous $FeCl_3$ solution, J. Sci. Arts. 1 (2010) 53–58. https://doi.org/10.1016/j.urolonc.2015.05.032.

[31] A. Mohammadi, M.-A. Hasan, B. Liedberg, I. Lundström, W.R. Salaneck, Chemical vapour deposition (CVD) of conducting polymers: Polypyrrole, Synth. Met. 14 (1986) 189–197. https://doi.org/https://doi.org/10.1016/0379-6779(86)90183-9.

[32] M. Totolin, M. Grigoraş, Plasma induced pyrrole polymerization, Rev. Roum. Chim. 52 (2007) 999–1005.

[33] J.Y. Kim, J.T. Kim, E.A. Song, Y.K. Min, H.O. Hamaguchi, Polypyrrole nanostructures self-assembled in magnetic ionic liquid as a template, Macromolecules. 41 (2008) 2886–2889. https://doi.org/10.1021/ma071333k.

[34] M.A. Chougule, S.G. Pawar, P.R. Godse, R.N. Mulik, S. Sen, V.B. Patil, Synthesis and Characterization of Polypyrrole (PPy) Thin Films, Soft Nanosci. Lett. 01 (2011) 6–10. https://doi.org/10.4236/snl.2011.11002.

[35] G. Inzelt, Conducting Polymers A New Era in Electrochemistry (Monographs in Electrochemistry), Springer, 2008.

[36] K. Leonavicius, A. Ramanaviciene, A. Ramanavicius, Polymerization Model for Hydrogen Peroxide Initiated Synthesis of Polypyrrole Nanoparticles, 27 (2011) 10970–10976. https://doi.org/10.1021/la201962a.

[37] S. Sadki, P. Schottland, N. Brodie, G. Sabouraud, S. Sa¨ıd, S. Dr, The mechanisms of pyrrole electropolymerization, Chem. Soc. Rev. 29 (2000) 283–293. https://doi.org/10.1039/a807124a.

[38] T.. Vernitskaya, Efimov O.N, Polypyrrole: a conducting polymer; its synthesis, properties and applications, Russ. Chem. Rev. 66 (1997) 443–457.

[39] D. Schmeisser, H. Naarmann, W. Göpel, The two-dimensional structure of polypyrrole films, Synth. Met. 59 (1993) 211–221. https://doi.org/10.1016/0379-6779(93)91028-Z.

[40] Y. Furukawa, S. Tazawa, Y. Fujii, I. Harada, Raman spectra of polypyrrole and its 2,5-13C-substituted and C-deuterated analogues in doped and undoped states, Synth. Met. 24 (1988) 329–341. https://doi.org/10.1016/0379-6779(88)90309-8.

[41] S.S. Shinde, G.S. Gund, D.P. Dubal, S.B. Jambure, C.D. Lokhande, Morphological modulation of polypyrrole thin films through oxidizing agents and their concurrent effect on supercapacitor performance, Electrochim. Acta. 119 (2014) 1–10. https://doi.org/10.1016/j.electacta.2013.10.174.

[42] K.G. Neoh, K.K.S. Lau, V.V.T. Wong, E.T. Kang, K.L. Tan, Structure and degradation behavior of polypyrrole doped with sulfonate anions of different sizes subjected to undoping-redoping cycles, Chem. Mater. 8 (1996) 167–172. https://doi.org/10.1021/cm950312e.

[43] J. Stejskal, M. Trchová, Conducting polypyrrole nanotubes: a review, Chem. Pap. 72

(2018) 1563–1595. https://doi.org/10.1007/s11696-018-0394-x.

[44] X. Chen, J. -P Issi, J. Devaux, D. Billaud, Chemically oxidized polypyrrole: Influence of the experimental conditions on its electrical conductivity and morphology, Polym. Eng. Sci. 35 (1995) 642–647. https://doi.org/10.1002/pen.760350803.

[45] D.P. Dubal, S.H. Lee, J.G. Kim, W.B. Kim, C.D. Lokhande, Porous polypyrrole clusters prepared by electropolymerization for a high performance supercapacitor, J. Mater. Chem. 22 (2012) 3044–3052. https://doi.org/10.1039/c2jm14470k.

[46] S. Paul, K.S. Choi, D.J. Lee, P. Sudhagar, Y.S. Kang, Factors affecting the performance of supercapacitors assembled with polypyrrole/multi-walled carbon nanotube composite electrodes, Electrochim. Acta. 78 (2012) 649–655. https://doi.org/10.1016/j.electacta.2012.06.088.

[47] K. Wang, H. Wu, Y. Meng, Z. Wei, Conducting polymer nanowire arrays for high performance supercapacitors, Small. 10 (2014) 14–31. https://doi.org/10.1002/smll.201301991.

[48] A.A. Kobets, E. V. Lobiak, G.K. Krivyakin, T. Kallio, E.O. Fedorovskaya, Function composition of modified reduced graphite oxide, Mater. Today Chem. 17 (2020) 100311. https://doi.org/10.1016/j.mtchem.2020.100311.

[49] T. Haisch, F. Kubannek, L. Nikitina, I. Nikitin, S. Pott, T. Clees, U. Krewer, The origin of the hysteresis in cyclic voltammetric response of alkaline methanol electrooxidation, Phys. Chem. Chem. Phys. 22 (2020) 16648–16654. https://doi.org/10.1039/d0cp00976h.

[50] J. Stejskal, I. Sapurina, M. Trchová, Polyaniline nanostructures and the role of aniline oligomers in their formation, Prog. Polym. Sci. 35 (2010) 1420–1481. https://doi.org/10.1016/j.progpolymsci.2010.07.006.

[51] I. Rodríguez, B.R. Scharifker, J. Mostany, In situ FTIR study of redox and overoxidation processes in polypyrrole films, J. Electroanal. Chem. 491 (2000) 117–125. https://doi.org/10.1016/S0022-0728(00)00194-7.

[52] A.A. Iurchenkova, E.O. Fedorovskaya, I.P. Asanov, V.E. Arkhipov, K.M. Popov, K.I. Baskakova, A. V. Okotrub, MWCNT buckypaper/polypyrrole nanocomposites for supercapasitor application, Electrochim. Acta. 335 (2020) 135700. https://doi.org/10.1016/j.electacta.2020.135700.

[53] R.G. Davidson, T.G. Turner, An IR spectroscopic study of the electrochemical reduction of polypyrrole doped with dodecylsulfate anion, Synth. Met. 72 (1995) 121–128. https://doi.org/10.1016/0379-6779(94)02332-S.

[54] H. Nguyen Thi Le, M.C. Bernard, B. Garcia-Renaud, C. Deslouis, Raman spectroscopy analysis of polypyrrole films as protective coatings on iron, Synth. Met. 140 (2004) 287–293. https://doi.org/10.1016/S0379-6779(03)00376-X.

[55] O.M. College, M.E. Road, L. El, Characterization of polypyrrole electropolyrnerized on different electrodes, Structure. 29 (1988) 1709–1717.

[56] Y. Furukawa, S. Tazawa, Y. Fujii, I. Harada, Raman spectra of polypyrrole and its 2,5-13C-substituted and C-deuterated analogues in doped and undoped states, Synth. Met.

24 (1988) 329–341. https://doi.org/10.1016/0379-6779(88)90309-8.

[57] M.J.L. Santos, A.G. Brolo, E.M. Girotto, Study of polaron and bipolaron states in polypyrrole by in situ Raman spectroelectrochemistry, Electrochim. Acta. 52 (2007) 6141–6145. https://doi.org/10.1016/j.electacta.2007.03.070.

[58] Y.C. Liu, B.J. Hwang, W.J. Jian, R. Santhanam, In situ cyclic voltammetry-surface-enhanced Raman spectroscopy: Studies on the doping-undoping of polypyrrole film, Thin Solid Films. 374 (2000) 85–91. https://doi.org/10.1016/S0040-6090(00)01061-0.

[59] P. Pfluger, G.B. Street, Chemical, electronic, and structural properties of conducting heterocyclic polymers: A view by XPS, J. Chem. Phys. 80 (1984) 544–553. https://doi.org/10.1063/1.446428.

[60] H. Ge, G. Qi, E.T. Kang, K.G. Neoh, Study of overoxidized polypyrrole using X-ray photoelectron spectroscopy, Polymer (Guildf). 35 (1994) 504–508. https://doi.org/10.1016/0032-3861(94)90503-7.

[61] L. Ruangchuay, J. Schwank, A. Sirivat, Surface degradation of α-naphthalene sulfonate-doped polypyrrole during XPS characterization, Appl. Surf. Sci. 199 (2002) 128–137. https://doi.org/10.1016/S0169-4332(02)00564-0.

[62] J. Tabačiarová, M. Mičušík, P. Fedorko, M. Omastová, Study of polypyrrole aging by XPS, FTIR and conductivity measurements, Polym. Degrad. Stab. 120 (2015) 392–401. https://doi.org/10.1016/j.polymdegradstab.2015.07.021.

[63] BEAMSON, G., High Resolution XPS of Organic Polymers, Sci. ESCA 300 Database. (1992). http://ci.nii.ac.jp/naid/10003489274/en/ (просмотрено 10 октябрь 2020 г.).

[64] S.N. Kumar, G. Bouyssoux, F. Gaillard, Electronic and structural characterization of electrochemically synthesized conducting polyaniline from XPS studies, Surf. Interface Anal. 15 (1990) 531–536. https://doi.org/10.1002/sia.740150906.

[65] K.L. Tan, B.T.G. Tan, E.T. Kang, K.G. Neoh, The chemical nature of the nitrogens in polypyrrole and polyaniline: A comparative study by x-ray photoelectron spectroscopy, J. Chem. Phys. 94 (1991) 5382–5388. https://doi.org/10.1063/1.460524.

[66] G. Ciric-Marjanovic, Recent advances in polyaniline research: Polymerization mechanisms, structural aspects, properties and applications, Synth. Met. 177 (2013) 1–47. https://doi.org/10.1016/j.synthmet.2013.06.004.

[67] A.A. Iurchenkova, E. V Lobiak, A.A. Kobets, A.N. Kolodin, A. Stott, S.R.P. Silva, E.O. Fedorovskaya, A complex study of the dependence of the re duce d graphite oxide electrochemical behavior on the annealing temperature and the type of electrolyte, 370 (2021). https://doi.org/10.1016/j.electacta.2021.137832.

[68] E. Frackowiak, F. Béguin, Carbon materials for the electrochemical storage of energy in capacitors, Carbon N. Y. 39 (2001) 937–950. https://doi.org/10.1016/S0008-6223(00)00183-4.

[69] E. Frackowiak, K. Metenier, V. Bertagna, F. Beguin, Supercapacitor electrodes from multiwalled carbon nanotubes, Appl. Phys. Lett. 77 (2000) 2421–2423. https://doi.org/10.1063/1.1290146.

[70] A.A. Kobets, A.A. Iurchenkova, I.P. Asanov, A.V. Okotrub, E.O. Fedorovskaya, Redox Processes in Reduced Graphite Oxide Decorated by Carboxyl Functional Groups, Phys. Status Solidi Basic Res. (2019). https://doi.org/10.1002/pssb.201800700.

[71] M.G. Sullivan, B. Schnyder, M. Bärtsch, D. Alliata, C. Barbero, R. Imhof, R. Kötz, Electrochemically Modified Glassy Carbon for Capacitor Electrodes Characterization of Thick Anodic Layers by Cyclic Voltammetry, Differential Electrochemical Mass Spectrometry, Spectroscopic Ellipsometry, X-Ray Photoelectron Spectroscopy, FTIR, and AFM, J. Electrochem. Soc. 147 (2000) 2636. https://doi.org/10.1149/1.1393582.

[72] C. Wu, J. Wang, Y. Bai, X. Li, Significant effect of cations on polypyrrole cycle stability, Solid State Ionics. 346 (2020) 115216. https://doi.org/https://doi.org/10.1016/j.ssi.2019.115216.

[73] A. V. Ivanishchev, I.A. Ivanishcheva, A. Dixit, LiFePO4-Based Composite Electrode Material: Synthetic Approaches, Peculiarities of the Structure, and Regularities of Ionic Transport Processes, Russ. J. Electrochem. 55 (2019) 719–737. https://doi.org/10.1134/S102319351908007X.

[74] Z. Zhang, Y. Zhang, X. Mu, J. Du, H. Wang, B. Huang, J. Zhou, X. Pan, E. Xie, The carbonization temperature effect on the electrochemical performance of nitrogen-doped carbon monoliths, Electrochim. Acta. 242 (2017) 100–106. https://doi.org/10.1016/j.electacta.2017.05.016.

[75] K.A. Owusu, L. Qu, J. Li, Z. Wang, K. Zhao, C. Yang, K.M. Hercule, C. Lin, C. Shi, Q. Wei, L. Zhou, L. Mai, Low-crystalline iron oxide hydroxide nanoparticle anode for high-performance supercapacitors, Nat. Commun. 8 (2017). https://doi.org/10.1038/ncomms14264.

[76] L. Liu, J. Lang, P. Zhang, B. Hu, X. Yan, Facile Synthesis of Fe2O3 Nano-Dots@Nitrogen-Doped Graphene for Supercapacitor Electrode with Ultralong Cycle Life in KOH Electrolyte, ACS Appl. Mater. Interfaces. 8 (2016) 9335–9344. https://doi.org/10.1021/acsami.6b00225.

[77] R. Li, J. Liu, Mechanistic investigation of the charge storage process of pseudocapacitive Fe3O4 nanorod film, Electrochim. Acta. 120 (2014) 52–56. https://doi.org/10.1016/j.electacta.2013.12.040.

[78] M. Sathiya, A.S. Prakash, K. Ramesha, J.M. Tarascon, A.K. Shukla, V2O5-anchored carbon nanotubes for enhanced electrochemical energy storage, J. Am. Chem. Soc. 133 (2011) 16291–16299. https://doi.org/10.1021/ja207285b.

[79] C. Zhong, Y. Deng, W. Hu, J. Qiao, L. Zhang, J. Zhang, A review of electrolyte materials and compositions for electrochemical supercapacitors, Chem. Soc. Rev. 44 (2015) 7484–7539. https://doi.org/10.1039/c5cs00303b.

[80] A. Ramanavicius, A. Finkelsteinas, H. Cesiulis, A. Ramanaviciene, Electrochemical impedance spectroscopy of polypyrrole based electrochemical immunosensor, Bioelectrochemistry. 79 (2010) 11–16. https://doi.org/10.1016/j.bioelechem.2009.09.013.

[81] H. Gul, A.-U.-H.A. Shah, U. Krewer, S. Bilal, Study on Direct Synthesis of Energy Efficient Multifunctional Polyaniline-Graphene Oxide Nanocomposite and Its

Application in Aqueous Symmetric Supercapacitor Devices. https://doi.org/10.3390/nano10010118.

[82] L. Jiang, J.A. Syed, Y. Gao, Q. Zhang, J. Zhao, H. Lu, X. Meng, Electropolymerization of camphorsulfonic acid doped conductive polypyrrole anti-corrosive coating for 304SS bipolar plates, Appl. Surf. Sci. 426 (2017) 87–98. https://doi.org/10.1016/j.apsusc.2017.07.077.

[83] A. Afzal, F.A. Abuilaiwi, A. Habib, M. Awais, S.B. Waje, M.A. Atieh, Polypyrrole/carbon nanotube supercapacitorsTechnological advances and challenges, J. Power Sources. 352 (2017) 174–186. https://doi.org/10.1016/j.jpowsour.2017.03.128.

[84] S.N.S. Goubert-Renaudin, X. Zhu, A. Wieckowski, Synthesis and characterization of carbon-supported transition metal oxide nanoparticles — Cobalt porphyrin as catalysts for electroreduction of oxygen in acids, Electrochem. commun. 12 (2010) 1457–1461. https://doi.org/https://doi.org/10.1016/j.elecom.2010.06.004.